

# Real-Time Evaluation of PMU-Based Fault Locators

F. V. Lopes, Y. M. P. Melo, D. Fernandes Jr., W. L. A. Neves

**Abstract**—In recent decades, the real-time fault location became an issue of great interest for electric utilities, since it contributes to a very fast post-fault power supply restoration, with no need to analyze oscillographic records. However, most of existing fault location algorithms are applied off-line to take advantages of more sophisticated procedures for error reducing. Here, four digital fault location methods typically applied off-line that are based on fundamental phasor values obtained through Phasor Measurement Units (PMU) were implemented in the Real Time Digital Simulator (RTDS) and compared among themselves. For this end, real-time digital simulations of faults on a 230 kV transmission line 300 km long were carried out and classical sources of errors such as inaccuracies in transmission line parameters, fault characteristics and the use of series compensation were addressed.

**Keywords:** Fault location, phasor measurement units, PMU-based methods, real-time, RTDS, transmission lines.

## I. INTRODUCTION

ELECTRIC power systems have grown rapidly in size and complexity over the last decades. Consequently, the length of transmission lines (TLs) increased, leading to greater chances of failures. As many utilities are operating in a deregulated environment and are competing with each other to increase the availability of power supply to the customers [1], fault locator devices have been proposed since 1950s to minimize power outage times due to short-circuits [2], [3].

Among the existing fault location methods, those based on fundamental-frequency phasors are the most commonly used in practice. In fact, they do not require high sampling frequency rates nor high computational efforts [1], what greatly improves their simplicity and cost. These techniques may be implemented using fundamental components computed by Phasor Measurement Units (PMUs), so that they are often refereed as PMU-based fault location algorithms.

Depending on the utilized input signals, PMU-based techniques can be classified in relation to the number of TL monitored terminals and to the availability of voltage and

current measurements [1]. Moreover, there exist in the literature approaches that consider phasors synchronized via Global Positioning System (GPS) [4]–[6] and that use unsynchronized data [7], [8]. In this context, it is known that most of these methods are typically applied off-line to take advantages of more sophisticated procedures which are able to improve the fault locator accuracy. Nevertheless, aiming to make power systems smarter, the on-line monitoring of TLs is becoming more and more important, in such a way that the real-time implementation and evaluation of fault location algorithms is nowadays an issue of great interest to electric utilities.

As the on-line fault location is a recent trend, there are not many works available in the state-of-the-art of power systems that report real-time analysis of classical fault location techniques. So, this paper aims to present details about the real-time implementation of digital fault location methods classically applied off-line and to evaluate their sensitivity to sources of errors like inaccuracies in TLs parameters, fault characteristics and the use of series capacitor banks with different degrees of compensation. For this end, the Real Time Digital Simulator (RTDS) [9] is used to simulate faults in a 230 kV TL 300 km long and to implement the evaluated methods. Altogether, four PMU-based fault location approaches are analyzed, including one- and two-terminal based algorithms.

## II. POWER SYSTEM NOTATION

The power system notation considered along this work is depicted in Fig. 1. Basically, it is analyzed a TL of length  $\ell$  which connects the sending-end (Bus S) to the receiving-end (Bus R).  $\widehat{V}_F$  is the fundamental voltage phasor at the fault point F, which is located at a distance of  $d$  km from the Bus S. On the other hand,  $\widehat{V}_S$ ,  $\widehat{I}_S$ ,  $\widehat{V}_R$  and  $\widehat{I}_R$  represent voltage and current phasors measured at buses S and R, whereas the Thévenin equivalent circuits S1 and S2 represent the power systems connected at each line terminal.

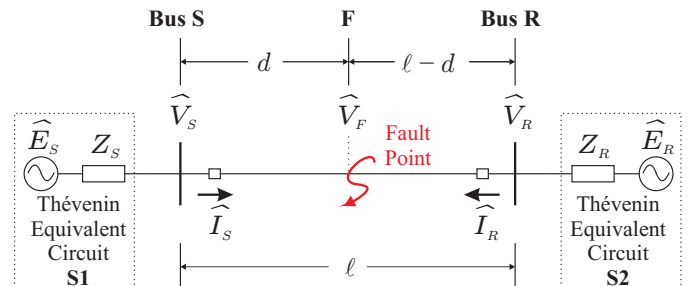


Fig. 1. Simulated power system single-line diagram.

This work was supported in part by the Brazilian National Council of Technological and Scientific Development (CNPq).

F. V. Lopes is a Ph.D. student at Federal University of Campina Grande (UFCG), 882 Aprígio Veloso Av., Bodocongó, 58.429-900, Campina Grande, PB, Brazil (e-mail: felipe.lopes@ee.ufcg.edu.br).

Y. M. P. Melo is a M. Sc. student at Federal University of Campina Grande (UFCG) (e-mail: yonatha.melo@ee.ufcg.edu.br).

D. Fernandes Jr. and W. L. A. Neves are with the Department of Electrical Engineering of Federal University of Campina Grande (UFCG) (e-mail: damasio@dee.ufcg.edu.br; waneves@dee.ufcg.edu.br).

Paper submitted to the International Conference on Power Systems Transients (IPST2013) in Vancouver, Canada July 18-20, 2013.

### III. EVALUATED PMU-BASED FAULT LOCATION ALGORITHMS

In this paper, four PMU-based fault location algorithms are evaluated, among which three methods are based on two terminal synchronized measurements and the remaining one is based on one-terminal data. The mathematical formulation of these techniques is presented next.

#### A. Method I: Proposed in [10]

A fault location approach based on one-terminal voltage and current data is presented in [10]. This type of method has been widely used by electric utilities due to its simplicity, low cost and mainly because it does not require communication channels to link both TL terminals nor the use of GPS for synchronizing phasor measurements.

In the Method I, input signals are selected in accordance to the faulted TL phases and to the presence of the ground on the fault, i.e., the fault classification is needed. Here, assuming that the fault type is known, six measurement units ( $Z_{AT}, Z_{BT}, Z_{CT}, Z_{AB}, Z_{BC}, Z_{CA}$ ) installed at the Bus S are used by the fault locator as presented in Table I [11], where  $\widehat{I}_0$  is the zero sequence current given by the sum of phase currents ( $\widehat{I}_0 = \widehat{I}_S^a + \widehat{I}_S^b + \widehat{I}_S^c$ ) and  $K_0$  is the residual compensation factor computed as follows:

$$K_0 = \frac{Z_{L0} - Z_{L1}}{Z_{L1}}, \quad (1)$$

where  $Z_{L0}$  and  $Z_{L1}$  are zero and positive sequence TL impedance, respectively.

As made in several fault location algorithms, Method I takes advantage of the additional information provided by the pre-fault currents seen by each measurement unit. Basically, the incremental current  $\Delta\widehat{I}_S$  is considered in order to minimize the load flow influence into the fault locator accuracy. This variable is obtained subtracting the stored pre-fault current value ( $\widehat{I}_p$ ) from its post-fault values ( $\widehat{I}_S$ ) and, then, used to compute the estimated fault distance  $d_{est}$ , in kilometers, such as follows:

$$d_{est} = \frac{\text{Im}\{\widehat{V}_S \Delta\widehat{I}_S^*\}}{\text{Im}\{Z_{L1} \widehat{I}_S \Delta\widehat{I}_S^*\}} \ell, \quad (2)$$

where  $\Delta\widehat{I}_S$  is the incremental current ( $\Delta\widehat{I}_S = \widehat{I}_S - \widehat{I}_p$ ) and (\*) is the conjugate function.

TABLE I  
METHOD I INPUT SIGNALS.

Measurement Unit	Voltage Signal* $\widehat{V}_S$	Current Signal* $\widehat{I}_S$
$Z_{AT}$	$\widehat{V}_S^a$	$\widehat{I}_S^a + K_0 \widehat{I}_0$
$Z_{BT}$	$\widehat{V}_S^b$	$\widehat{I}_S^b + K_0 \widehat{I}_0$
$Z_{CT}$	$\widehat{V}_S^c$	$\widehat{I}_S^c + K_0 \widehat{I}_0$
$Z_{AB}$	$\widehat{V}_S^a - \widehat{V}_S^b$	$\widehat{I}_S^a - \widehat{I}_S^b$
$Z_{BC}$	$\widehat{V}_S^b - \widehat{V}_S^c$	$\widehat{I}_S^b - \widehat{I}_S^c$
$Z_{CA}$	$\widehat{V}_S^c - \widehat{V}_S^a$	$\widehat{I}_S^c - \widehat{I}_S^a$

\*The superscripts  $a, b$  and  $c$  represent TL phases.

#### B. Method II: Proposed in [4]

The algorithm proposed in [4] is considered as one of the most accurate available in the literature, as it takes into account the line shunt capacitance during the fault location procedure. In summary, by knowing voltage and current phasors at the Bus S, it is possible to derive an expression that can be used to compute the voltage phasor at any point of the TL located at a distance  $x$  from the sending-end such as follows:

$$\widehat{V}(x) = \widehat{V}_S \cosh(\gamma x) - \widehat{I}_S Z_C \sinh(\gamma x). \quad (3)$$

The same analysis may be performed considering data from the Bus R, what results in an expression for the voltage phasor at any point of the TL located at a distance  $y$  from the receiving-end.

$$\widehat{V}(y) = \widehat{V}_R \cosh(\gamma y) - \widehat{I}_R Z_C \sinh(\gamma y). \quad (4)$$

Using (3) and (4) to calculate the voltage phasor  $\widehat{V}_F$  at the fault point F, we obtain:

$$\widehat{V}_F = \widehat{V}(x) \Big|_{x=d} = \widehat{V}(y) \Big|_{y=\ell-d}. \quad (5)$$

Substituting (3) and (4) in (5) and taking the variable  $d$  as the estimated fault location  $d_{est}$ , we can derive that:

$$d_{est} = \frac{\tanh^{-1}(-B/A)}{\gamma}, \quad (6)$$

being

$$A = Z_C \widehat{I}_S - \widehat{V}_R \sinh(\gamma \ell) + Z_C \widehat{I}_R \cosh(\gamma \ell), \quad (7)$$

and

$$B = \widehat{V}_R \cosh(\gamma \ell) - Z_C \widehat{I}_R \sinh(\gamma \ell) - \widehat{V}_S, \quad (8)$$

where  $Z_C$  is the TL surge impedance given by

$$Z_C = \sqrt{\frac{R + j\omega L}{G + j\omega C}}, \quad (9)$$

and  $\gamma$  the line propagation constant computed as follows:

$$\gamma = \sqrt{(R + j\omega L)(G + j\omega C)}, \quad (10)$$

where  $\omega = 2\pi f$  is the angular power frequency,  $f$  is the power frequency and  $R, L, G$  and  $C$  are the TL series resistance, series inductance, shunt conductance and shunt capacitance, per unit length, respectively.

Originally, the algorithm presented in [4] uses voltage and current modal quantities, so that the fault type classification is needed for properly selecting the excited aerial-mode component. However, it is known that symmetrical quantities can also be applied for the case of three-phase fully transposed TLs [3], in such way that the positive sequence component is always excited irrespective of the fault type. Hence, for simplicity, being the TL modeled here transposed, the Method II is implemented using only positive sequence signals, avoiding the necessity to recognize the fault type.

### C. Method III: Proposed in [5]

A two-terminal fault location algorithm is proposed in [5] for the case of TLs monitored at two or three points, using synchronized or unsynchronized measurements. In this work, only the version that considers two-terminal synchronized data is analyzed, since it is the most widespread in the literature.

The Method III is formulated from the voltage phasor  $\widehat{V}_F$  computation, taking into account only the series TL impedance. Thus, by knowing phasors  $\widehat{V}_S$ ,  $\widehat{I}_S$ ,  $\widehat{V}_R$  and  $\widehat{I}_R$ , (11) and (12) are derived, where  $Z_{abc}$  is the series TL impedance matrix per unit length,  $V_F^{abc}$  is the voltage vector of phasors at the fault point and  $V_S^{abc}$ ,  $V_R^{abc}$ ,  $I_S^{abc}$  and  $I_R^{abc}$  are the voltage and current vectors of phasors measured at buses S and R.

$$V_F^{abc} = V_S^{abc} - dZ_{abc}I_S^{abc}, \quad (11)$$

$$V_F^{abc} = V_R^{abc} - (\ell - d)Z_{abc}I_R^{abc}. \quad (12)$$

From (11) and (12), (13) is derived:

$$V_S^{abc} - V_R^{abc} + \ell Z_{abc}I_R^{abc} = dZ_{abc}(I_S^{abc} + I_R^{abc}), \quad (13)$$

which can be rewritten as:

$$Y = M \cdot d \quad \text{or} \quad \begin{bmatrix} Y_a \\ Y_b \\ Y_c \end{bmatrix} = \begin{bmatrix} M_a \\ M_b \\ M_c \end{bmatrix} \cdot d, \quad (14)$$

being

$$M_j = \sum_{i=a,b,c} Z_{ji}(\widehat{I}_S^i + \widehat{I}_R^i), \quad \text{for } j = a,b,c, \quad (15)$$

$$Y_j = \widehat{V}_S^j - \widehat{V}_R^j + \ell \sum_{i=a,b,c} (Z_{ji}\widehat{I}_R^i), \quad \text{for } j = a,b,c. \quad (16)$$

According to [5], (14) may be solved using the least-square estimates and, so, taking  $d$  as the estimated fault distance  $d_{est}$ , the fault location can be determined by:

$$d_{est} = (M^+M)^{-1}M^+Y, \quad (17)$$

where  $M^+$  is the conjugate transpose of  $M$ .

In this paper, the TL series impedance matrix  $Z_{abc}$  is calculated from the zero and positive sequence TL parameters such as suggested in [12] and following described:

$$Z_{abc} = \begin{bmatrix} Z_{aa} & Z_{ab} & Z_{ac} \\ Z_{ba} & Z_{bb} & Z_{bc} \\ Z_{ca} & Z_{cb} & Z_{cc} \end{bmatrix} = \begin{bmatrix} Z_S & Z_M & Z_M \\ Z_M & Z_S & Z_M \\ Z_M & Z_M & Z_S \end{bmatrix}, \quad (18)$$

where  $Z_M = (Z_{L0} - Z_{L1})/3$ ,  $Z_S = Z_M + Z_{L1}$ ,  $Z_S$  is the TL self impedance,  $Z_M$  is the TL mutual impedance and, finally,  $Z_{L0}$  and  $Z_{L1}$  represent zero and positive sequence impedances assuming that the TL is completely transposed.

### D. Method IV: Proposed in [6]

This fourth method is proposed in [6]. This technique is also based on synchronized phasor measurements at two terminals of the monitored line and, unlike the other algorithms described so far, it does not require the knowledge of TL parameters. Such feature greatly improves the fault locator reliability in the field, where TL sequence data values normally present inaccuracies.

According to the formulation depicted in [6], the fault distance may be calculated from the analysis of positive and negative sequence voltage and current phasors at both TL ends. Thus, being the superscripts 'p' and 'n' respectively related to the positive and negative sequence components, we can obtain:

$$\widehat{V}_S^p - Z_{L1}d\widehat{I}_S^p = \widehat{V}_R^p - Z_{L1}(\ell - d)\widehat{I}_R^p, \quad (19)$$

$$\widehat{V}_S^n - Z_{L1}d\widehat{I}_S^n = \widehat{V}_R^n - Z_{L1}(\ell - d)\widehat{I}_R^n, \quad (20)$$

where  $\ell$  and  $Z_{L1}$  are, respectively, the line length and the positive sequence TL series impedance.

Aiming on the elimination of TL parameters from the algorithm expressions, the computation of terms  $dZ_{L1}$  and  $(\ell - d)Z_{L1}$  is proposed. Thus, being

$$dZ_{L1} = \frac{(\widehat{V}_S^p - \widehat{V}_R^p)\widehat{I}_R^n - (\widehat{V}_S^n - \widehat{V}_R^n)\widehat{I}_R^p}{\widehat{I}_S^p\widehat{I}_R^n - \widehat{I}_S^n\widehat{I}_R^p}, \quad (21)$$

$$(\ell - d)Z_{L1} = \frac{(\widehat{V}_S^p - \widehat{V}_R^p)\widehat{I}_S^n - (\widehat{V}_S^n - \widehat{V}_R^n)\widehat{I}_S^p}{\widehat{I}_S^p\widehat{I}_R^n - \widehat{I}_S^n\widehat{I}_R^p}, \quad (22)$$

the fault distance from the Bus S, per unit length, may be represented by:

$$d(\text{p.u.}) = \frac{d}{\ell} = \frac{dZ_{L1}}{dZ_{L1} + (\ell - d)Z_{L1}}. \quad (23)$$

Substituting (21) and (22) in (23) and taking  $d$  as the estimated fault location  $d_{est}$ , the fault distance can be estimated, in kilometers, using:

$$d_{est} = \frac{(\widehat{V}_S^p - \widehat{V}_R^p)\widehat{I}_R^n - (\widehat{V}_S^n - \widehat{V}_R^n)\widehat{I}_R^p}{(\widehat{V}_S^p - \widehat{V}_R^p)(\widehat{I}_S^n + \widehat{I}_R^n) - (\widehat{V}_S^n - \widehat{V}_R^n)(\widehat{I}_S^p + \widehat{I}_R^p)} \ell. \quad (24)$$

It is important to point out that in such a hypothetical case in which the line parameters are known with no error, the estimated fault distance  $d_{est}$  is a pure real value [4]. However, in practice, for methods that use TL data,  $d_{est}$  values normally present a quite small imaginary part due to inaccuracies that commonly exist in line parameters. Thus, in this work, all evaluated methods consider the fault location as the real part of  $d_{est}$  such as suggested in [4].

## IV. REAL-TIME IMPLEMENTATION OF PMU-BASED FAULT LOCATION METHODS

For the real-time evaluation of methods I, II, III and IV, a simplified PMU was implemented using tools available in the RTDS like the *Draft Interface* and the *Cbuilder Module* [9]. The modeled PMU contains anti-aliasing filters, analog to digital (A/D) converters, phasor estimators and symmetrical component estimators, so that it provides all input signals for the analyzed fault location algorithms as depicted in the flowchart shown in Fig. 2.

The simulation time step of the RTDS is  $50 \mu\text{s}$ , what leads to voltage and current waveforms composed by 333 samples per cycle for a power frequency of 60 Hz. Here, we consider such signals as the "analog" three-phase primary voltages and currents, which are transformed to the secondary voltage and current waveforms through potential and current transformer models available in the *Draft Interface* of the RTDS. These secondary signals are then forwarded to the PMU block, whose parts are described in the next subsections.

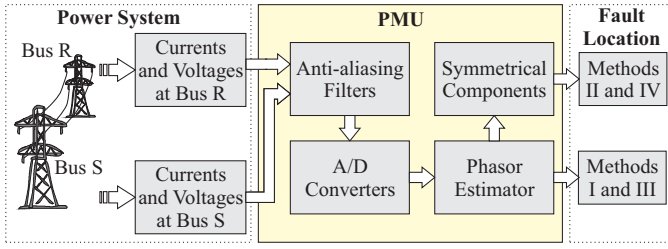


Fig. 2. Simplified PMU flowchart.

### A. Anti-aliasing filters and A/D converters (or down-samplers)

The anti-aliasing filter is an analog low-pass filter with a cut-off frequency less than or equal to one-half of the sampling rate used by the A/D converter [13]. In this work, since only fundamental frequency components (60 Hz) are needed, "analog" secondary signals are sampled at a rate of 960 Hz (16 samples/cycle), so that low-pass third order Butterworth filters with a cut-off frequency of 180 Hz are used. Fig. 3(a) depicts the functional blocks used to implement the anti-aliasing filters and the A/D converters.

One can see that A/D converters are simulated using down-samplers. As aforementioned, the primary analog voltage and current waveforms are represented here by digital signals with 333 samples/cycle, so that the down-sampling procedure into secondary signals is enough to simulate a simplified A/D conversion. Also, from Fig. 3(a), it is observed the existence of a trigger signal, whose status is changed whenever a new set of voltage and current samples are available at each TL terminal, starting the phasor estimation step described next.

### B. Phasor estimation

The phasor estimation algorithm used in this work is the Modified Cosine Filter (MCF), which is presented in [14]. The MCF operations are implemented here using the *Cbuilder Module* for a 16 samples/cycle sampling rate, what resulted in the phasor estimator block shown in Fig. 3(b).

The phasor estimator inputs are the secondary waveform samples, whereas its outputs are the real and imaginary parts of voltage and current phasors. The frequency responses of MCF real and imaginary parts are depicted in Fig. 4, where the convolution of the MCF outputs with the frequency response of the modeled anti-aliasing filter is also shown.

Since the MCF algorithm is based on data windows of one power frequency cycle, all harmonics are filtered (Fig. 4). Furthermore, the anti-aliasing filters minimize the side lobes of the real and imaginary filter parts, further improving the off-nominal frequency component filtering. It is important to point out that the MCF algorithm also attenuates the decaying DC component, leading to a faster stabilization of fundamental phasors after the fault inception. Even so, the fault location is computed in this work picking up phasor values five cycles after the disturbance beginning, when the DC component influence can be considered negligible [15].

As depicted in Fig. 2, methods I and III directly use the MCF outputs to locate faults. However, methods II and IV use symmetrical components, which are computed here such as described in the next subsection.

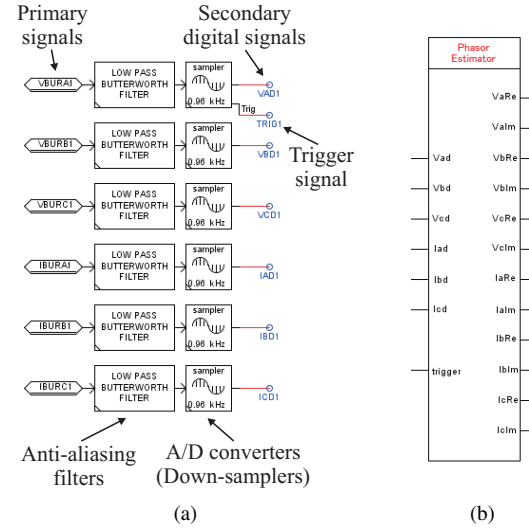


Fig. 3. PMU modules: (a) Anti-aliasing filters and A/D converters; (b) Phasor estimator.

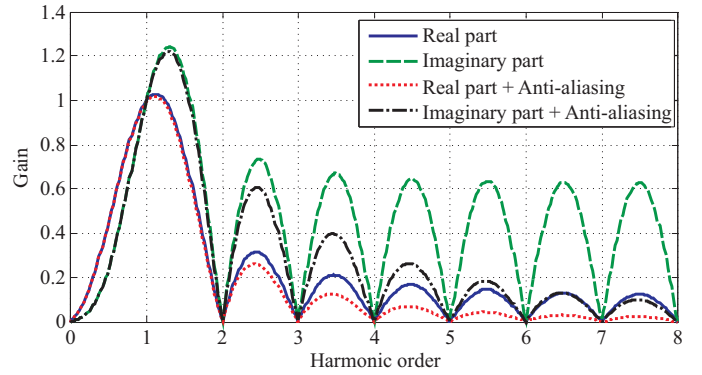


Fig. 4. Magnitude of the MCF real and imaginary parts frequency response.

### C. Computation of symmetrical components

In this step, positive and negative sequence quantities are computed in order to provide the input signals of methods II and IV. Being the modeled TL completely transposed, a linear transformation from phase components to a set of symmetrical components [1], as for example for the sending-end voltage  $\hat{V}_S$ , is performed according to:

$$\begin{bmatrix} \hat{V}_S^0 \\ \hat{V}_S^p \\ \hat{V}_S^n \end{bmatrix} = [T_s]^{-1} \cdot \begin{bmatrix} \hat{V}_S^a \\ \hat{V}_S^b \\ \hat{V}_S^c \end{bmatrix}, \quad (25)$$

being

$$[T_s] = \begin{bmatrix} 1 & 1 & 1 \\ 1 & \alpha^2 & \alpha \\ 1 & \alpha & \alpha^2 \end{bmatrix}, \quad (26)$$

where  $\alpha = e^{j2\pi/3} = 1 \angle 120^\circ$ , and the superscripts 'p', 'n' and '0' respectively denote the positive, negative and zero sequence components.

To compute symmetrical quantities, complex functions already available in the RTDS *Draft Interface* in the library *Controls/Complex Math Functions* were used. After this step, all evaluated fault location methods are enabled and their outputs are monitored. The main difficulties to implement such PMU-based fault locators are briefly discussed next.

## D. Fault Location and Implementation Difficulties

The evaluated fault location algorithms are predominantly implemented in this work using complex functions available in the RTDS *Draft Interface*. However, some difficulties have been encountered during the Method II implementation. This algorithm requires hyperbolic functions able to receive complex inputs, which are not available in the simulator libraries.

To overcome the aforementioned problem, the *CBuilder Module* was used to develop the required math functions. Basically, the real and imaginary parts of the  $\sinh()$ ,  $\cosh()$  and  $\tanh^{-1}()$  were formulated for the case of using complex inputs and, then, embedded into new control blocks. Even so, in spite of such difficulties, it should be pointed out that, in general, all methods have presented very simple real-time implementations.

## V. REAL-TIME SIMULATIONS

To evaluate methods I, II, III and IV, RTDS fault simulations are performed and then, the percentage errors  $\epsilon$  of the estimated fault point in each studied case is computed using:

$$\epsilon(\%) = \frac{|d - d_{est}|}{\ell} \times 100, \quad (27)$$

where  $d$  and  $d_{est}$  are the actual and the estimated fault distance, respectively.

The modeled 230 kV power system is the one depicted in Fig. 1, whose parameters are shown in Table II. In the evaluation, the fault distance  $d$  is made to vary from 10% to 90% of the line length  $\ell$  with steps of 5%, while fault resistances  $R_f$ , fault type, inaccuracies into TL data and the series compensation degrees are changed depending on the analysis. The TL is modeled as a fully transposed line, using a constant distributed-parameter line model. Also, the existence of a communication channel linking both TL terminals and of a GPS for synchronizing data is considered.

## A. Fault Type Effect

For the fault type effect analysis, evaluated methods are applied to locate faults with  $R_f = 0.01 \Omega$  assuming that the TL parameters are known with no error. From Fig. 5, it is observed that methods I, II and III are robust to the fault type, being the performance of the one-terminal technique (Method I) influenced by the fault distance. Moreover, one can see that Method IV present overall good results, with the exception of those related to three-phase faults, when errors of about 4% are found. In fact, besides the positive sequence components, Method IV uses the negative sequence quantities, which in turn do not exist for ABC faults.

## B. Fault Resistance Effect

In order to evaluate the fault resistance effect, AG faults are simulated, assuming that there are no inaccuracies into TL data. As depicted in Fig. 6, only the one-terminal technique (Method I) is strongly affected by  $R_f$ , what is in accordance to other papers presented in the literature [3], [16]. On the other hand, two-terminal algorithms (methods II, III and IV) present negligible performance variations for the different  $R_f$  values. It attests that two-terminal fault locators have a significant robustness to the fault resistance.

TABLE II  
POWER SYSTEM PARAMETERS.

Equivalent Circuit S1	Equivalent Circuit S2
$\hat{E}_S = 1.02 \angle 0^\circ$ p.u.	$\hat{E}_R = 0.98 \angle -10^\circ$ p.u.
$Z_{S0} = 18.78 \angle 86.91^\circ \Omega$	$Z_{R0} = 20.87 \angle 86.90^\circ \Omega$
$Z_{S1} = 25.67 \angle 89.81^\circ \Omega$	$Z_{R1} = 28.53 \angle 88.06^\circ \Omega$
Transmission Line ( $\ell = 300$ km)	
$Z_{L0} = 0.522 + j1.432 \Omega/\text{km}$	$Z_{L1} = 0.098 + j0.53 \Omega/\text{km}$
$Y_{L0} = 2.293 \mu\text{S}/\text{km}$	$Y_{L1} = 3.252 \mu\text{S}/\text{km}$

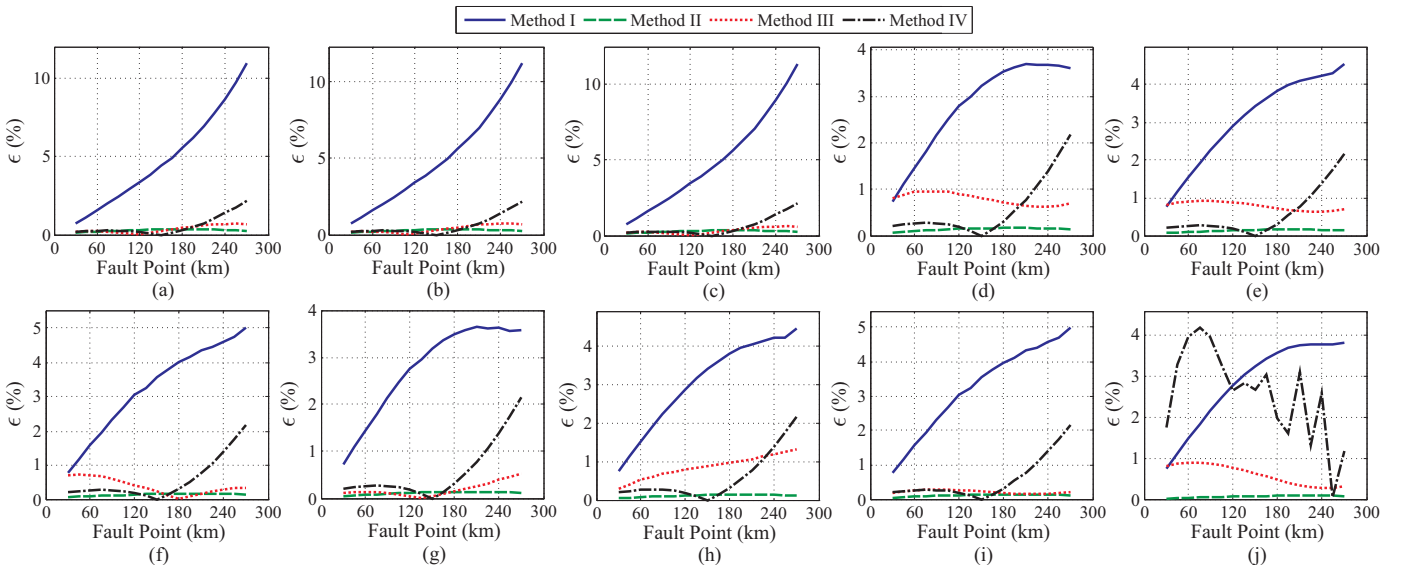


Fig. 5. Fault type effect: (a) AG; (b) BG; (c) CG; (d) AB; (e) BC; (f) AC; (g) ABG; (h) BCG; (i) ACG; (j) ABC.

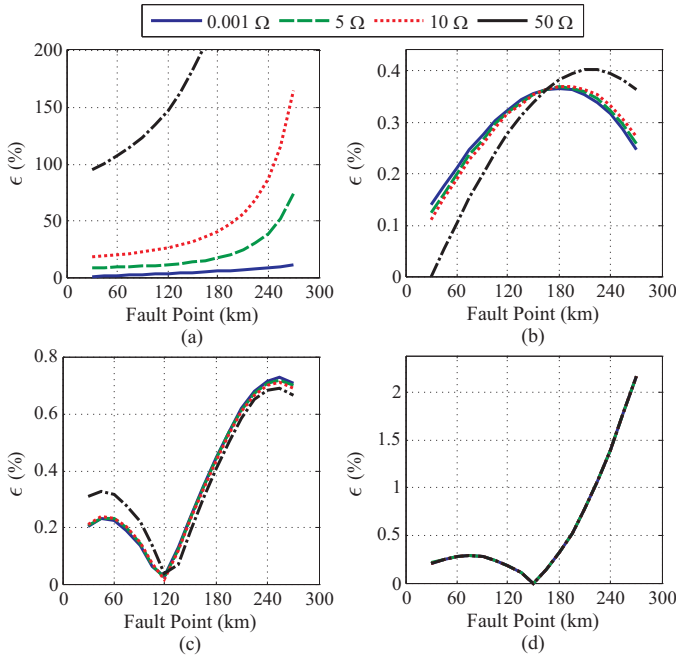


Fig. 6. Fault resistance effect: (a) Method I; (b) Method II; (c) Method III; (d) Method IV.

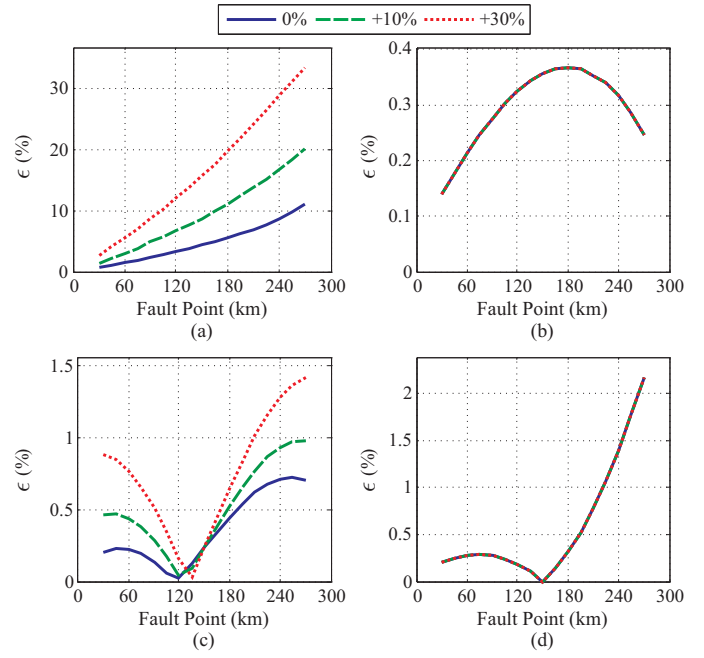


Fig. 7. Effect of inaccuracies into zero sequence TL parameters: (a) Method I; (b) Method II; (c) Method III; (d) Method IV.

### C. Effect of Inaccuracies into TL Parameters

In practice, the computation of TL parameters is a difficult task, as they differ with the loading and weather conditions [6]. Thus, inaccuracies into line data frequently lead to relevant fault location errors, which is very undesirable. In this work, we decide to analyze zero sequence inaccuracies  $\Delta Z_{L0}$  of about +10% and +30% as well as positive sequence deviations  $\Delta Z_{L1}$  of -30%, -10%, +10% and +30%. In order to do so, AG faults with  $R_f = 0.01 \Omega$  are analyzed.

Obtained results are shown in Figs. 7 and 8. One can see that methods II and IV are not influenced by  $\Delta Z_{L0}$ , whereas methods I and III are affected. Even so, it should be pointed out that only the one-terminal technique lead to unacceptable fault location errors, so that the Method III can be also considered as robust to zero sequence data deviations.

Analyzing now the influence of  $\Delta Z_{L1}$ , one can notice that the Method III is slightly affected and that the Method IV is completely robust to such TL data inaccuracy. It highlights the significant robustness of both techniques. On the other hand, methods I and II are influenced by inaccuracies into positive sequence TL parameters. Considering the performance of the Method II, it is verified that the greater the  $\Delta Z_{L1}$  in magnitude, the greater the fault location error. As a result,  $\epsilon$  values higher than 6% are verified for  $\Delta Z_{L1} = -30\%$ . This is an important result, since such technique is the one which presented the best performance in the evaluation tests discussed so far. Besides, in relation to the Method I, results show that in some cases, depending on the  $\Delta Z_{L1}$  value, the fault locator performance can be improved for faults close to the Bus R. Even so, in general, it may be observed that the fault location accuracy is compromised by  $\Delta Z_{L1}$ , so that the influence of such inaccuracies is quite undesirable.

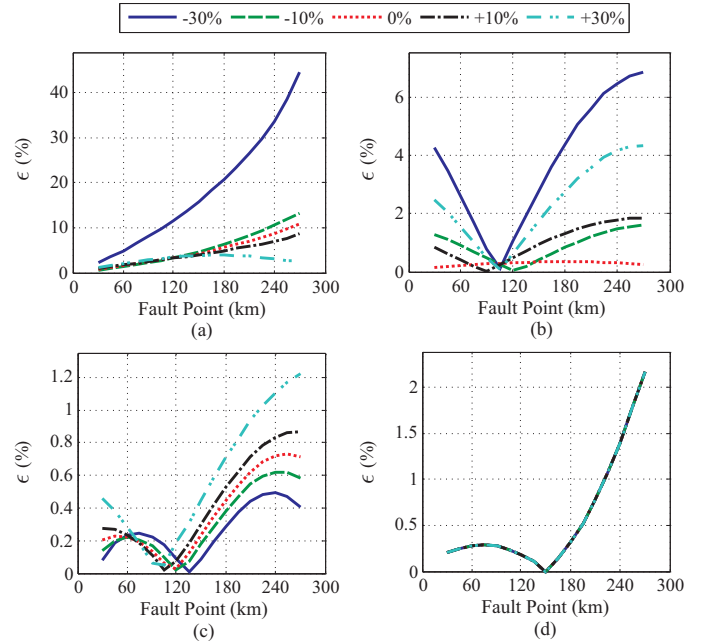


Fig. 8. Effect of inaccuracies into positive sequence TL parameters: (a) Method I; (b) Method II; (c) Method III; (d) Method IV.

### D. Series Compensation Effect

Series compensated TLs utilize series capacitor banks to cancel a portion of the line inductive reactance [17]. It improves various line operational features such as its power transmission capability, voltage regulation and stability. Although this type of compensation has been widely applied in transmission networks, the use of series capacitor banks is known to create problems in control and protection systems, as well as in PMU-based fault locators. To investigate such effects, AG faults with  $R_f = 0.01 \Omega$  are analyzed here considering capacitor banks installed at the Bus S side.

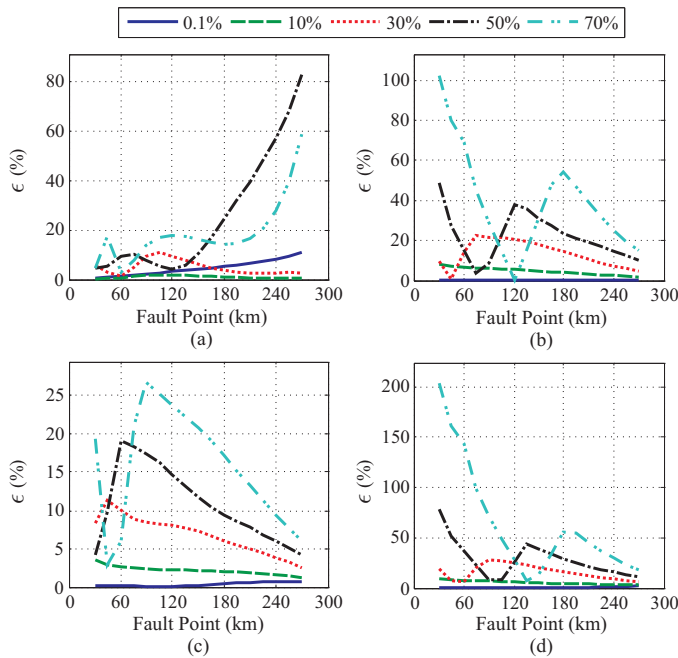


Fig. 9. Series compensation effect: (a) Method I; (b) Method II; (c) Method III; (d) Method IV.

In the literature, there are available some techniques which were designed specifically to locate faults on series compensated TLs [1]. Thus, our main objective is only to show that evaluated methods I, II, III and IV cannot be directly applied to such type of line, unless extra procedures are added. Fig. 9 depicts the obtained results for compensation degrees (CDs) of 0.01%, 10%, 30%, 50% and 70%.

One can notice that all evaluated techniques are affected by the series compensation, so that unacceptable fault location errors are found (errors of about a few tens of kilometers) for CDs up to 10%. This is due to potential differences across the capacitors, which are included into analyzed voltages that are measured here at the bus side. However, these errors can be minimized using the line side voltages, if they are available, instead of the bus side signals. Another simple solution is to analytically compensate the voltage drop across the capacitors such as described in [18]. Even so, it requires the knowledge of the series capacitances, so that if they are not known, methods I, II, III and IV can not be applicable.

## VI. CONCLUSIONS

In this paper, one- and two-terminal PMU-based fault location methods typically applied off-line were evaluated in real-time. For this purpose, a simplified PMU containing anti-aliasing filters, A/D converters, a phasor estimation algorithm and a symmetrical component estimator was modeled using the RTDS tools and, then, real-time simulations of faults on a 230 kV TL 300 km long were studied, addressing the influence of sources of errors like inaccuracies in TL parameters, fault characteristics and the use of series compensation. Difficulties encountered for implementing the evaluated fault location algorithms in the RTDS were also commented.

As expected, the effects of the fault resistance and the fault distance can be practically eliminated by using two-terminal

fault location methods, even though one-terminal ones are still the most simple to be implemented in the field. Besides, results highlighted the influence of the series compensation, which may lead the algorithms to completely diverge. So, excluding the compensated TL case for which there exist special methods, one can conclude about the implemented approaches that the two-terminal algorithms are very accurate and reliable, being in some cases robust even to inaccuracies in TL parameters. In future works, we intend to investigate the influence of other important sources of error like errors in estimated fundamental phasors and in the synchronism between the local and remote data.

## VII. ACKNOWLEDGMENT

The authors would like to thank the Brazilian National Research Council (CNPq) for the financial support of this research.

## VIII. REFERENCES

- [1] M. M. Saha, J. Izykowski, and E. Rosolowski, *Fault Location on Power Networks*, ser. Power Systems. London: Ed. Springer, 2010.
- [2] T. W. Stringfield, D. J. Marihart, and R. F. Stevens, "Fault location methods for overhead lines," *Transactions of the American Institute of Electrical Engineers Power Apparatus and Systems, Part III.*, vol. 76, no. 3, pp. 518–529, april 1957.
- [3] A. Dalcastagne and S. Zimath, "A study about the sources of error of impedance-based fault location methods," in *2008 IEEE/PES Transmission and Distribution Conference and Exposition: Latin America*, aug. 2008, pp. 1–6.
- [4] A. Johns and S. Jamali, "Accurate fault location technique for power transmission lines," *IEE Proceedings C Generation, Transmission and Distribution*, vol. 137, no. 6, pp. 395–402, Nov. 1990.
- [5] A. Girgis, D. Hart, and W. Peterson, "A new fault location technique for two- and three-terminal lines," *IEEE Transactions on Power Delivery*, vol. 7, no. 1, pp. 98–107, Jan. 1992.
- [6] Z. M. Radojevic, C. H. Kim, M. Popov, G. Preston, and V. Terzija, "New approach for fault location on transmission lines not requiring line parameters," *International Conference on Power Systems Transients*, Jun. 2009.
- [7] J. Izykowski, E. Rosolowski, P. Balcerek, M. Fulczyk, and M. Saha, "Accurate noniterative fault location algorithm utilizing two-end unsynchronized measurements," *IEEE Transactions on Power Delivery*, vol. 25, no. 1, pp. 72–80, jan. 2010.
- [8] C.-S. Yu, "An unsynchronized measurements correction method for two-terminal fault-location problems," *IEEE Transactions on Power Delivery*, vol. 25, no. 3, pp. 1325–1333, july 2010.
- [9] *Real Time Digital Simulator Tutorial Manual*, RTDS Technologies Inc., Winnipeg, Manitoba, Canada, 2008.
- [10] T. Takagi, Y. Yamakoshi, M. Yamaura, R. Kondow, and T. Matsushima, "Development of a new type fault locator using the one-terminal voltage and current data," *IEEE Transactions on Power Apparatus and Systems*, vol. PAS-101, no. 8, pp. 2892–2898, Aug. 1982.
- [11] G. Ziegler, *Numerical Distance Protection: Principles and Applications*. Berlin, Germany: Siemens, 2010.
- [12] H. W. Dommel, *Electromagnetic Transients Program Reference Manual: EMTP Theory Book*, Portland, BPA, 1996.
- [13] A. G. Phadke and J. S. Thorp, *Computer Relaying for Power Systems*, 2nd ed. New York, USA: John Wiley & Sons Inc, 2009.
- [14] D. G. Hart, D. Novosel, and R. A. Smith, *Modified Cosine Filters*, U. S. Patent 6154687 ed., November, 2000.
- [15] G. Benmouyal, "Removal of dc-offset in current waveforms using digital mimic filtering," *IEEE Transaction on Power Delivery*, vol. 10, no. 2, pp. 621–630, Apr. 1995.
- [16] M. Hashim, H. W. Ping, and V. Ramachandaramurthy, "Impedance-based fault location techniques for transmission lines," in *TENCON 2009 - 2009 IEEE Region 10 Conference*, jan. 2009, pp. 1–6.
- [17] P. M. Anderson, *Power System Protection*. Piscataway, NJ - USA: IEEE Press Series on Power Engineering, 1999.
- [18] E. O. Schweitzer, "A review of impedance-based fault locating experience," *Fourteenth Annual Iowa-Nebraska System Protection Seminar*, oct. 1990.